

# Optical Detection of Early Damage in Retinal Ganglion Cells in a Mouse Model of Partial Optic Nerve Crush Injury

Ji Yi,<sup>\*,1</sup> Zhen Puyang,<sup>2,3</sup> Liang Feng,<sup>3</sup> Lian Duan,<sup>1</sup> Peiji Liang,<sup>2</sup> Vadim Backman,<sup>1</sup> Xiaorong Liu,<sup>3,4</sup> and Hao F. Zhang<sup>1,3</sup>

<sup>1</sup>Department of Biomedical Engineering, Northwestern University, Evanston, Illinois, United States

<sup>2</sup>School of Biomedical Engineering, Shanghai Jiao Tong University, Shanghai, China

<sup>3</sup>Department of Ophthalmology, Northwestern University, Chicago, Illinois, United States

<sup>4</sup>Department of Neurobiology, Northwestern University, Evanston, Illinois, United States

Correspondence: Xiaorong Liu, Hogan 2-160, 2205 Tech Drive, Evanston, IL 60208, USA; xiaorong-liu@northwestern.edu. Hao F. Zhang, Biomedical Engineering Department, Northwestern University, 2145 Sheridan Road, Evanston, IL 60208, USA; hfzhang@northwestern.edu.

JY and ZP contributed equally to the work presented here and should therefore be regarded as equivalent authors.

Current affiliation: \*Department of Medicine, Boston University School of Medicine, Boston, Massachusetts, United States

Submitted: May 18, 2016

Accepted: September 7, 2016

Citation: Yi J, Puyang Z, Feng L, et al. Optical detection of early damage in retinal ganglion cells in a mouse model of partial optic nerve crush injury. *Invest Ophthalmol Vis Sci*. 2016;57:5665-5671. DOI:10.1167/iovs.16-19955

**PURPOSE.** Elastic light backscattering spectroscopy (ELBS) has exquisite sensitivity to the ultrastructural properties of tissue and thus has been applied to detect various diseases associated with ultrastructural alterations in their early stages. This study aims to test whether ELBS can detect early damage in retinal ganglion cells (RGCs).

**METHODS.** We used a mouse model of partial optic nerve crush (pONC) to induce rapid RGC death. We confirmed RGC loss by axon counting and characterized the changes in retinal morphology by optical coherence tomography (OCT) and in retinal function by full-field electroretinogram (ERG), respectively. To quantify the ultrastructural properties, elastic backscattering spectroscopic analysis was implemented in the wavelength-dependent images recorded by reflectance confocal microscopy.

**RESULTS.** At 3 days post-pONC injury, no significant change was found in the thickness of the RGC layer or in the mean amplitude of the oscillatory potentials measured by OCT and ERG, respectively; however, we did observe a significantly decreased number of axons compared with the controls. At 3 days post-pONC, we used ELBS to calculate the ultrastructural marker ( $D$ ), the shape factor quantifying the shape of the local mass density correlation functions. It was significantly reduced in the crushed eyes compared with the controls, indicating the ultrastructural fragmentation in the crushed eyes.

**CONCLUSIONS.** Elastic light backscattering spectroscopy detected ultrastructural neuronal damage in RGCs following the pONC injury when OCT and ERG tests appeared normal. Our study suggests a potential clinical method for detecting early neuronal damage prior to anatomical alterations in the nerve fiber and ganglion cell layers.

**Keywords:** ganglion cells, spectroscopy, optical coherence tomography, electroretinography, axonal degeneration

Optic neuropathy (or retinal neuropathy) is often characterized by the loss of or damage to the optic nerves that leads to retinal ganglion cell (RGC) death and vision impairments.<sup>1,2</sup> One of the earliest recognized manifestations of optic neuropathy is the ultrastructural alteration in the axon or the body of RGCs.<sup>3</sup> It has been reported that a myriad of molecular alterations observed in early-stage RGC/axon damage result in ultrastructural changes, including DNA fragmentation, axon disruption, and mitochondria swelling, among others.<sup>3,4</sup> Although beyond the optical diffractive limit, these ultrastructural alterations collectively change the optical-scattering properties in tissue. Thus, optical detection that is sensitive to ultrastructural alterations in the nerve fiber layer (NFL)/RGC layer can be an effective method for identifying the early onset of optic neuropathy.

Elastic light backscattering spectroscopy (ELBS) has demonstrated extraordinary sensitivity to ultrastructural alterations at a length scale of tens of nanometers in tissue without actually resolving the nanoarchitecture.<sup>5-8</sup> Elastic light backscattering spectroscopy has been used to detect various cancers at early

stages, even in “histologically normal” precancerous lesions.<sup>9,10</sup> The measured spectroscopic biomarkers were found to be associated with some ubiquitous structural hallmarks in cancers such as enlarged nuclear sizes, chromatin compaction, and extracellular matrix crosslinking.<sup>11,12</sup> Using backscattering light to detect structural abnormalities in retina, Huang et al.<sup>13,14</sup> pioneered the work showing that wavelength-dependent scattering changes occur in NFL in elevated intraocular pressure (IOP) rat and murine models, and revealed that the optical changes were linked to cytoskeleton distortion.

In this study we investigated whether ELBS can be used to detect earlier biomarkers of NFL/RGC damage compared with other morphologic and functional methods/techniques. We induced rapid RGC death by partial optic nerve crush injury in mice.<sup>15</sup> The damage to the optic nerve was verified by the gradual decrease of axon density. The consequential functional and morphologic changes were quantified by ERG and optical coherence tomography (OCT). The spectroscopic markers were quantified by analyzing the wavelength-dependent scattering signals measured by confocal reflectance microsc-



py. We found that the spectroscopic changes in the backscattered light can be observed at the very early stage of RGC death, prior to the detectable functional and morphologic alterations.

## MATERIALS AND METHODS

All animal procedures were approved by the institutional animal care and use committee at Northwestern University and conformed with the guidelines on the Use of Animals from the National Institutes of Health and the ARVO Statement for the Use of Animals in Ophthalmic and Vision Research.

### Partial Optic Nerve Crush (pONC) Procedure

First, C57BL/6J mice (Jackson laboratory, Bar Harbor, ME, USA) were anesthetized with an intraperitoneal injection of ketamine (100 mg/kg; Lloyd, Inc., Shenandoah, IA, USA) and xylazine (10 mg/kg; Butler Schein Animal Health, Dublin, OH, USA). The surgery of the partial optic nerve crush was as described in Puyang et al.<sup>15</sup> In brief, a small incision was made in the superior and lateral conjunctiva, and a gentle blunt dissection was performed to expose the optic nerve using fine forceps (Dumont #5B, WPI, Sarasota, FL, USA). The optic nerve was partially clamped with self-closing forceps (WPI) for 3 s/site approximately 0.5 to 1 mm behind the globe.<sup>15</sup> The superior and temporal area was thus defined as the crush-operated (CO) side, and the inferior and nasal area as the nonoperated (NO) side.

### Optical Coherence Tomography

The system has been described in detail in previous publications.<sup>16,17</sup> Briefly, we used a super continuum light source (SuperK EXW-6; NKT Photonics, Birkerød, Denmark) to provide visible-light illumination from 520 to 620 nm, which permitted a higher axial resolution than OCT systems operating within near-infrared light spectral range. The illuminating light was delivered by an optical fiber, collimated by a lens, and input into a cube beam splitter (BS, CMI-BS013; Thorlabs, Inc., Newton, NJ, USA), by which the light was divided into a sample arm and a reference arm. The sample arm consisted of a two-dimensional scanning mirror and a 1:5 telescope system. A line scan CCD camera (sp2k; Basler Electric, Highland, IL, USA) was used to record the spectrum in a custom-made spectrometer; the exposure rate was 25 kHz with the exposure time 37  $\mu$ s. The three-dimensional (3D) image took 2.62 seconds, consisting of  $256 \times 256$  pixels in two lateral directions. The lateral resolution was determined by diffraction-limited focus spot and subjected to aberration in the eye. The axial and lateral resolution of our system was estimated as  $\sim 1.8 \mu$ m and 15  $\mu$ m in air, respectively.

We took the axial dimension of the first bright layer beneath the retinal inner-limiting membrane as the thickness of the NFL and ganglion cell layer (GCL) and measured this value manually in each high-definition OCT image.<sup>18,19</sup> For each retina, we took 15 to 25 measurements in the cross-section images with definable boundary using ImageJ (<http://imagej.nih.gov/ij/>; provided in the public domain by the National Institutes of Health, Bethesda, MD, USA). The thickness of the NFL and GCL was measured separately at the CO and NO sites following pONC injury.

### Full Field Electroretinogram Recording

Full-field ERG recording was performed with an ERG system (Micron III; Phoenix Research Labs, Pleasanton, CA, USA) as

described previously.<sup>20</sup> In brief, animals were dark-adapted overnight and anesthetized before experiments. The electrical response was elicited by 10 ms of flash spot with a diameter of 2050  $\mu$ m. Multiple light intensities ( $-2.0, -0.97, 0.51, 2.13$ , and  $3.53 \log \text{scot cd/m}^2$ ) were applied to each eye. Electroretinogram data were analyzed using customized software (MATLAB; MathWorks, Natick, MA, USA) and amplitudes of oscillatory potentials (OPs) were measured to evaluate the inner retinal function.<sup>20</sup>

### Confocal Reflectance Microscopy

Mice were perfused with 4% paraformaldehyde fixation and eyes were then enucleated. A blue mark was made on the superior quadrant to indicate the orientation. The anterior chamber, ocular lens, and vitreous were carefully removed. The exposed eye cup was immersed in PBS for 15 minutes. The retina was then carefully removed from the choroid and flat-mounted on a glass slide with PBS as the mounting medium. Confocal reflectance microscopic images were taken by a microscope system (Leica SP5; Leica Microsystems, Inc., Wetzlar, Germany). The focus was set on to the NFL with the depth of focus  $\sim 6 \mu$ m, which is determined by the pinhole size (Fig. 1A). The illumination wavelength swept from 470 to 670 nm by 10-nm intervals, resulting in 21 wavelength-dependent images (Fig. 1B). The spectral fluctuation in the scattering intensity was compensated by taking a reflectance image from a clear glass surface with the same condition. The normalized spectra were fitted with a power law function based on a spectral model of  $\lambda^{D-4}$ , as illustrated in Figure 1C. The modeling is described in detail in the next section.

### Analytical Model for ELBS Analysis

Macromolecules are the fundamental building blocks of living cells. Based on the Gladstone-Dale equation, the tissue's refractive index (RI) is proportional to the local macromolecular mass density<sup>21,22</sup>:

$$n = n_0 + \rho\alpha, \quad (1)$$

where  $\rho$  (g/mL) is the local mass density of the solid material (e.g., macromolecules),  $\alpha$  (mL/g) is the RI increment, usually approximately 0.17 mL/g for biological materials<sup>23,24</sup>; and  $n_0$  is the RI of water. The heterogeneous distribution of mass density causes RI fluctuation, which leads to detectable backscattered light due to elastic scattering.

Because of the heterogeneous nature of the mass density distribution, we modeled tissue as a random medium with continuously fluctuating mass density. The most comprehensive way to describe such a medium is by its correlation function (i.e., mass density correlation function).<sup>25-27</sup> We used a three-parameter functional family, the Whittle-Matérn (WM) function, to quantify the correlation functional form.<sup>28</sup> This versatile functional family covers essentially all of the commonly used correlation functions, including the power law, exponential, stretched exponential, and the Gaussian function. The functional family of WM is formulated as<sup>11</sup>:

$$B_n(r_d) = A_n \left( \frac{r_d}{L_n} \right)^{(D-3)/2} K_{(D-3)/2} \left( \frac{r_d}{L_n} \right), \quad (2)$$

where  $K_{l,j}$  is a modified Bessel function of the second type,  $A_n$  is the amplitude of the RI fluctuation,  $D$  is the "shape factor" determining the type of the function,<sup>27</sup> and  $L_n$  is the length scale of the correlation function whose exact meaning depends on  $D$ . When  $0 < D < 3$ , the correlation function can be described by a power law and the tissue is organized as a fractal.<sup>25</sup> Given the linear relationship between RI and mass

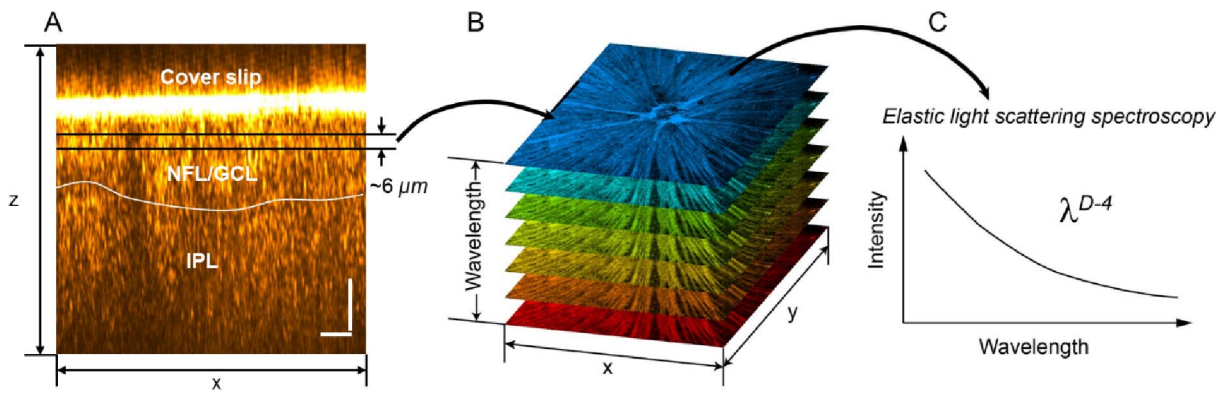


**FIGURE 1.** Ultrastructural quantification using ELBS. (A, B) Wavelength-dependent confocal reflectance en face images were taken from flat-mounted retinas ex vivo. The focus was adjusted within the neural fiber layer and ganglion cell layer beneath the cover slip. (C) At each pixel of the en face images, the spectrum was fitted by a power law equation with an exponent of  $4 - D$ ;  $D$  defines the autocorrelation function of ultrastructural mass density distribution.

density,  $D$  is the mass density fractal dimension  $D_m$ . When  $3 < D < 4$ , the functional form becomes a stretched exponential function. For  $D = 4$ ,  $B_n(r_d)$  is an exponential function, where  $B_n(L_n) = B_n(0)^{-1}$ . When  $D$  approaches infinity, the function turns into a Gaussian form.

The first-order Born approximation can be used to predict the scattering power spectral density  $\Phi$  by the Fourier transform of  $B_n(r_d)$ ,  $\Phi(k) = FT(B_n)$ .<sup>6,28</sup> Then, the differential cross-section per-unit volume  $\sigma(\theta, \phi)$  can be analytically expressed, where  $\theta$  and  $\phi$  denote the scattering angle in a spherical coordinate with respect to the incident direction. Since confocal reflectance detects the backscattered light, the light intensity is proportional to the backscattering coefficient  $\mu_b$ . The conditioned function of  $\mu_b$  is<sup>11,29,30</sup>:

$$\mu_b = A_n 2^{\left(\frac{D}{2} + 1\right)} \pi^{\frac{3}{2}} \Gamma\left(\frac{D}{2}\right) L_n^{3-D} k^{4-D}, \quad kL_n \gg 1, \quad (3)$$

where  $\Gamma$  is the gamma function. According to Equation 3, the backscattering spectrum is a power law function to  $k$  where the exponent is equal to  $4 - D$ . Because  $k$  is equal to  $2\pi/\lambda$ , the confocal reflectance spectrum follows  $\lambda^{D-4}$  where the exponent becomes  $D - 4$  with respect to wavelength. By fitting the spectrum with a power law function,  $D$  can inversely be calculated.

### Axon Counting

A cross-section of the proximal optic nerve was prepared as described previously.<sup>31</sup> In brief, the optic nerves were fixed in glutaraldehyde in resin (EOPN-Araldite; Electron Microscopy Sciences, Hatfield, PA, USA) and cut into 1- $\mu$ m sections. The sections were then stained with p-phenylenediamine (Sigma-Aldrich Corp., St. Louis, MO, USA) and imaged under an inverted microscope (Carl Zeiss Microscopy LLC, Thornwood, NY, USA). The axon numbers per image were counted using ImageJ, averaged, and then normalized to the total area of the optic nerve.<sup>31</sup>

### Statistics

We used two sample student's  $t$ -tests to calculate the statistical significance. For electroretinogram, 2-way ANOVA was used to examine the influence of two independent variables (time point and light intensity). For spectroscopic analysis from the confocal measurements, the paired  $t$ -test was used to calculate the statistical difference between the operated eye and the fellow eye from the same subjects.

## RESULTS

We used a pONC model to induce rapid RGC and axon loss.<sup>15</sup> First, we evaluated the retinal morphological changes by in vivo OCT (Figs. 2A–C). We took OCT images from the mouse retinas before crush, and at 3 days and 1 week postcrush ( $n = 5$  for each group). The thickness of NFL + GCL was measured separately in selected regions from the inferior and nasal side (referred as the nonoperated side) and the crush-operated (CO) side in high-resolution cross-sectional OCT images (Figs. 2A, 2B). At 3 days post-pONC injury, no significant decrease in NFL + GCL thickness was observed compared with the control mice ( $n = 5$ ,  $P > 0.05$  in student's  $t$ -test; Fig. 2C). At 1 week postcrush injury, the thickness of NFL + GCL decreased in both areas (NO:  $15 \pm 1 \mu\text{m}$ , CO:  $14 \pm 1 \mu\text{m}$ ,  $n = 5$ ,  $P < 0.001$  in student's  $t$ -test; Fig. 2C). Interestingly, damage was found in the entire retina (i.e., both CO and NO areas). No significant difference between NO and CO was observed in NFL + GCL thickness ( $P > 0.05$  in student's  $t$ -test, Fig. 2C).

We performed scotopic full-field ERG recordings to examine functional changes during the first week following the crush injury. Our data suggested the mean amplitude of OPs, which reflects the inner retinal function, was not significantly reduced ( $n = 5$  in each group,  $P < 0.001$  in 2-way ANOVA with Tukey's posttest; Fig. 2D) until 1 week postcrush. At 3 days postcrush, we only observed the trend of decrease in the OPs, but the change was not significant ( $n = 5$ ,  $P > 0.05$  in 2-way ANOVA with posttest; Fig. 2D). These results demonstrated a robust reduction in visual responses from the inner retina at 1 week postcrush injury, consistent with our morphologic findings.

We next examined the degeneration of optic nerve at 3 days postcrush in fixed tissues. The optic nerve samples from the controls and the mice at 3 days postcrush were dissected, fixed, and cryosectioned (see "Methods" section). In the cross-sections of optic nerves from the control mice, axons appeared as dark circles of myelin surrounding unstained axoplasm (Fig. 2E). We observed the disruption of the myelin sheath, hyperdense axoplasm, and vacuolization in the images taken from 3 days postcrush groups. In addition, glial reaction was activated and resulted in numerous large, lipid-containing glial scars (Fig. 2E).<sup>15</sup> We counted the total number of axons from both groups. For the control eyes, the mean axon number was  $46,463 \pm 1358$  ( $n = 9$ ). For the 3 days postinjury group, the total axon number was substantially reduced to  $28,990 \pm 1930$  ( $n = 4$ ,  $P < 0.001$  in student's  $t$ -test; Fig. 2F). Together our data suggest there is a significant reduction in axon number, though

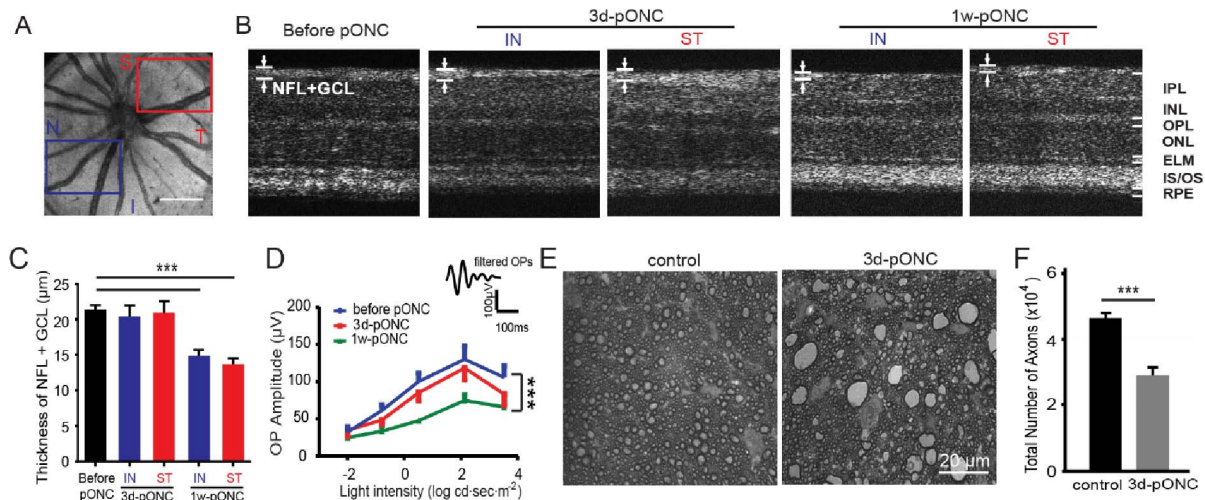


**FIGURE 2.** Characterization of retinal damage by OCT, ERG, and axon counting post-pONC injury. (A–C) Imaging of OCT detected a significant reduction in the NFL + GCL thickness at 1 week but not 3 days post-pONC injury. (A) Example of en face projection of 3D OCT from a mouse retina in vivo. Areas of CO (red) and NO (blue) were labeled. I, inferior; N, nasal; S, superior; T, temporal. Scale bar: 0.4 mm. (B) Representative cross-sectional OCT images of mouse retinas. ELM, external limiting membrane; INL, inner nuclear layer; IPL, inner plexiform layer; IS/OS: inner segment/outer segment; ONL, outer nuclear layer; OPL, outer plexiform layer. (C) The thickness of NFL + GCL before pONC, 3 days and 1 week post-pONC. Areas of NO and CO were measured separately post-pONC;  $n = 5$  mice for each group. \*\*\*  $P < 0.001$  in student's  $t$ -tests. (D) Mean amplitudes of OPs before crush, at 3 days and 1 week post-pONC. Example of a filtered OP was shown as an inset. \*\*\*  $P < 0.001$  in student's  $t$ -tests. (E) Representative micrographs of optic nerve sections in a control and a 3-day postcrush eye. (F) Total axon numbers were quantified ( $n = 9$  in control,  $n = 4$  in 3 days). \*\*\*  $P < 0.001$  in Student's  $t$ -tests.

the change may not be detected by in vivo OCT and ERG at 3 days postinjury.

Having characterized the morphologic and functional changes in retina, we then investigated whether the optical spectroscopic marker can be a more sensitive indicator of NFL/RGC damage. We calculated the values of  $D$  (i.e., the “shape factor” defining the functional type of the mass density autocorrelation function) within 3 days postinjury, when neither NFL/RGC thickness nor ERG showed significant differences between injured and control eyes. Figure 3A shows an example of the averaged spectra from the injured (left) and

control (right) eyes. The injured retina has a reflectance spectrum that decreases faster at longer wavelengths, indicating a lower  $D$ , and also has more fragmented ultrastructures. When we overlaid the  $D$  values onto the grayscale confocal reflectance images, as shown in Figure 3B, it exhibited overall lower  $D$  3 days postcrush compared with the control retina. It also appeared that  $D$  was lower near the optic nerve head, indicating that the damage was propagating from the optic disk. Statistically, the reduction of  $D$  is significant (control:  $D = 4.0 \pm 0.2$ ; CO:  $D = 3.56 \pm 0.3$ ,  $n = 10$  animals,  $P = 0.001$  paired student's  $t$ -test), as shown in Figure 3C. We also

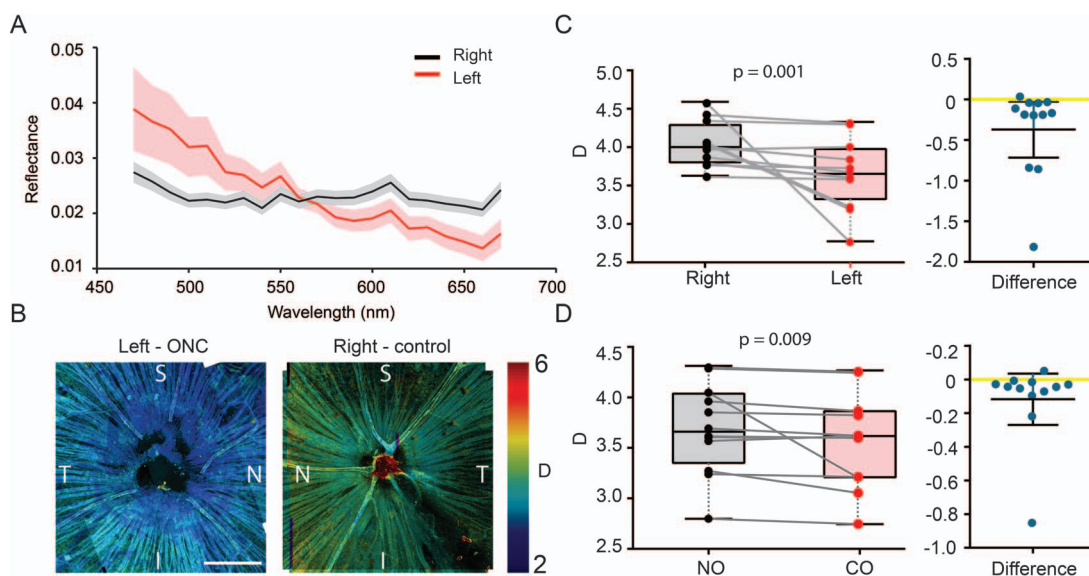


**FIGURE 3.** Ex vivo ultrastructural quantification of early NFL damage. (A) Examples of reflectance spectrum from a left (ONC) and right (control) eye. The shaded areas showed the standard errors. (B) Representative confocal reflectance images of flat-mounted retinas from left (ONC) and right (control) eye from the same animal.  $D$  was pseudocolor-encoded on the images. (C–D) Paired comparison of  $D$  between left (ONC) and right (control) eyes, and between NO quadrants and CO quadrants;  $n = 10$  mice.

compared the NO and CO (superior temporal side of retina) regions, where a reduction of  $D$  also was observed (CO:  $D = 3.56 \pm 0.32$ ; NO:  $D = 3.5 \pm 0.35$ ,  $n = 10$  retinas,  $P = 0.009$  paired student's  $t$ -test, as shown in Figure 3D. We noticed that data vary significantly among different animals, but the paired difference between two eyes from the same animals showed constant  $D$  reduction. The intersubject  $D$  variance could arise from the inconsistency of perfusion fixing, in which each animal may have been fixed slightly differently.

## DISCUSSION

In this study we tested whether the ultrastructural marker  $D$  obtained by ELBS can be an early indicator for NFL/RGC damage. We introduced acute axon damage by pONC in mice, which propagated to the retina and caused RGC death. We found that neither NFL/RGL thickness nor ERG OP amplitude showed significant changes within 3 days post-pONC, while there is significant reduction of ultrastructural marker  $D$  from the injured eye compared with the fellow eye from the same animals, as well as from the crushed site compared with the noncrushed site.

The spectroscopic analysis that was used to calculate  $D$  is rooted from the tissue's ultrastructural properties. The fundamental origin of this elastic optical backscattering is the RI fluctuation within tissue. Based on the Gladstone-Dale equation, tissue RI is linearly proportional to the local macromolecular mass density<sup>22</sup>; thus, the measurement of backscattered light allows us to quantify the native tissue structures. Because of the heterogeneous nature of the tissue, we can use the mass density autocorrelation function to describe the tissue structures and establish a model where  $D$  quantifies the shape of the autocorrelation function. Conceptually, a more condensed structure will yield higher  $D$  than a more fragmented structure. More importantly, it has been theoretically and experimentally shown that the length-scale sensitivity by measuring  $D$  can reach as low as 40 nm, beyond the diffraction-limited resolution of any ophthalmic imaging modality.<sup>30,32</sup> In this study, we observed lower  $D$  values from NFL/GCL in crushed eye, indicating more fragmented ultrastructures. This result aligns well with the previous finding that DNA fragmentation and cell disintegration occurs in the early stage of RGC damage, as well as the disruption of cytoskeleton.<sup>3</sup>

Interestingly, we observed that the overall change of  $D$  across all quadrants compared with the control was greater than that of the crushed quadrant compared with the nonoperated quadrants. This suggests that secondary effects may exist in the ultrastructure to the entire retina in response to the nerve crush. This could also be evident by the propagation of the optic nerve damage. Secondary degeneration of RGCs, which has been found in pONC or transection models of different animals,<sup>33-36</sup> could be caused by the deleterious molecules released from the RGCs or glial cells damaged by the primary direct insults. First, oxidative stress, calcium overload, or mitochondrial dysfunction in the primarily injured RGCs could produce or regulate proapoptotic signals to neighboring RGCs,<sup>33,35,37,38</sup> causing the DNA fragmentation and cell disintegration. Second, retinal glial cells such as microglia, astrocytes, and oligodendrocytes also played a role in the secondary degeneration after pONC,<sup>39,40</sup> which may also contribute to the  $D$  change observed here; however, the specific mechanisms of these complex pathologies need further study.<sup>41,42</sup>

The reflectance spectroscopic contrast in NFL has been previously studied by Huang et al.<sup>13</sup> In their study, an elevated IOP rat model was used to introduce global damage

to the NFL. Using a multispectral imaging microreflectometer, the spectroscopic contrast was found between the glaucomatous and the control eyes. A neural fiber bundle model was used to elucidate the structural mechanism, where the loss of the thin neural fiber bundles from the simulation underpinned their experimental observations.<sup>13,14</sup> In our study, we focused on investigating longitudinally whether an ultrastructural marker can be used to detect early NFL damage by comparing it with the morphological marker (NFL thickness) and the functional markers (OP amplitude) measured at the same time point. We used confocal gating by confocal reflectance microscopy to collect the reflected light from a  $\sim 6$   $\mu\text{m}$ -thick tissue layer, which was mostly composed of NFLs reflection and partially reflected from soma toward periphery. We adopted a continuous RI fluctuating model to interpret our observation. The model suggests the ultrastructural fragmentation within NFL/RGCs. This fragmentation also may contribute to the loss of neural fiber bundles previously found by Huang et al.<sup>13</sup>

This paper presents a proof-of-concept study for using ELBS for early detection of optic neuropathy. For in vivo measurements, the ultrastructural marker  $D$  can be measured and derived using other ophthalmologic imaging modalities that provide depth discrimination on the retina. For example, hyperspectral adaptive optics scanning laser ophthalmoscopy potentially could be used to provide spectroscopic measurement from NFL/RGCs layers.<sup>43,44</sup> Optical coherence tomography, which is the standard of care in morphologic ophthalmic imaging, could also provide depth-resolved spectroscopic measurements. We recently demonstrated a novel OCT method to quantify  $D$  values locally through spectroscopic analysis,<sup>27</sup> which could potentially translate this study into clinical and preclinical in vivo applications.

The limitation of this study is the possible influence of the fixation process on the tissue's ultrastructures. The fixatives denature proteins and introduce crosslinking to preserve the structure while at the same time could in principle increase the  $D$  values.<sup>11,45</sup> However, the advantage of fixation is more rigorous control over the confocal microscopic measurements between the crushed and normal retinas, and the significant difference of the ultrastructural marker still can be observed in the current study. Future in vivo measurement of retinal ultrastructure from intact retinas is work in progress.

## Acknowledgments

The authors thank the Northwestern University Atomic and Nanoscale Characterization Experimental Center (NUANCE) for preparation of optic nerve sections.

Supported by National Institutes of Health Grants R01EY026286 (XL); DP3DK108248 (HFZ); and R01CA183101 (VB); the National Science Foundation CBET-1055379 (HFZ); a National Natural Science Foundation of China Grant No. 31471054 (PL); and a Program of Introducing Talents of Discipline to Universities Grant No. B08020 (PL).

Disclosure: **J. Yi**, None; **Z. Puyang**, None; **L. Feng**, None; **L. Duan**, None; **P. Liang**, None; **V. Backman**, NanoCytomics (I); **X. Liu**, None; **H.F. Zhang**, Opticent Health (I)

## References

- Behbehani R. Clinical approach to optic neuropathies. *Clin Ophthalmol*. 2007;1:233-246.
- Buono LM, Foroozan R. Perioperative posterior ischemic optic neuropathy: review of the literature. *Surv Ophthalmol*. 2005; 50:15-26.
- Barron KD, Dentinger MP, Krohel G, Easton SK, Mankes R. Qualitative and quantitative ultrastructural observations on

- retinal ganglion cell layer of rat after intraorbital optic nerve crush. *J Neurocytol.* 1986;15:345-362.
4. Carelli V, Ross-Cisneros FN, Sadun AA. Mitochondrial dysfunction as a cause of optic neuropathies. *Prog Retin Eye Res.* 2004;2:53-89.
  5. Boustany NN, Boppart SA, Backman V. Microscopic imaging and spectroscopy with scattered light. *Annu Rev Biomed Eng.* 2010;512:285-314.
  6. Rogers JD, Radosevich AJ, Yi J, Backman V. Modeling light scattering in tissue as continuous random media using a versatile refractive index correlation function. *IEEE J Sel Top Quantum Electron.* 2013;20:7000514.
  7. Cherkezyan L, Capoglu I, Subramanian H, et al. Interferometric spectroscopy of scattered light can quantify the statistics of subdiffractional refractive-index fluctuations. *Phys Rev Lett.* 2013;111:033903.
  8. Hunter M, Backman V, Popescu G, et al. Tissue self-affinity and polarized light scattering in the Born approximation: a new model for precancer detection. *Phys Rev Lett.* 2006;97:138102.
  9. Backman V, Roy HK. Advances in biophotonics detection of field carcinogenesis for colon cancer risk stratification. *J Cancer.* 2013;4:251-261.
  10. Chalut KJ, Ostrander JH, Giacomelli MG, Wax A. Light scattering measurements of subcellular structure provide noninvasive early detection of chemotherapy-induced apoptosis. *Cancer Res.* 2009;69:1199-1204.
  11. Yi J, Radosevich AJ, Stypula-Cyrus Y, et al. Spatially resolved optical and ultrastructural properties of colorectal and pancreatic field carcinogenesis observed by inverse spectroscopic optical coherence tomography. *J Biomed Opt.* 2014;19:36013.
  12. Yi J, Stypula-Cyrus Y, Blaha CS, Roy HK, Backman V. Fractal characterization of chromatin decompaction in live cells. *Biophys J.* 2015;109:2218-2226.
  13. Huang XR, Zhou Y, Knighton RW, Kong W, Feuer WJ. Wavelength-dependent change of retinal nerve fiber layer reflectance in glaucomatous retinas. *Invest Ophthalmol Vis Sci.* 2012;53:5869-5876.
  14. Huang XR, Zhou Y, Kong W, Knighton RW. Reflectance decreases before thickness changes in the retinal nerve fiber layer in glaucomatous retinas. *Invest Ophthalmol Vis Sci.* 2011;52:6737-6742.
  15. Puyang Z, Feng L, Chen H, Liang P, Troy JB, Liu X. Retinal ganglion cell loss is delayed following optic nerve crush in NLRP3 knockout mice. *Sci Rep.* 2016;6:20998.
  16. Yi J, Wei Q, Liu W, Backman V, Zhang HF. Visible-light optical coherence tomography for retinal oximetry. *Opt Lett.* 2013;38:1796-1798.
  17. Chen S, Yi J, Zhang HF. Measuring oxygen saturation in retinal and choroidal circulations in rats using visible light optical coherence tomography angiography. *Biomed Opt Express.* 2015;6:2840-2853.
  18. Huber G, Beck SC, Grimm C, et al. Spectral domain optical coherence tomography in mouse models of retinal degeneration. *Invest Ophthalmol Vis Sci.* 2009;50:5888-5895.
  19. Ruggeri M, Wehbe H, Jiao S, et al. In vivo three-dimensional high-resolution imaging of rodent retina with spectral-domain optical coherence tomography. *Invest Ophthalmol Vis Sci.* 2007;48:1808-1814.
  20. Chen H, Zhao Y, Liu M, et al. Progressive degeneration of retinal and superior collicular functions in mice with sustained ocular hypertension degeneration of visual functions in glaucoma. *Invest Ophthalmol Vis Sci.* 2015;56:1971-1984.
  21. Barer R, Tkaczyk S. Refractive index of concentrated protein solutions. *Nature.* 1954;173:821-822.
  22. Davies HG, Wilkins MHF, Chayen J, La Cour LE. The use of the interference microscope to determine dry mass in living cells and as a quantitative cytochemical method. *Q J Microsc Sci.* 1954;(s3-95):271-304.
  23. Cherkezyan L, Subramanian H, Stoyneva V, et al. Targeted alteration of real and imaginary refractive index of biological cells by histological staining. *Opt Lett.* 2012;37:1601-1603.
  24. Zhao H, Brown PH, Schuck P. On the distribution of protein refractive index increments. *Biophys J.* 2011;100:2309-2317.
  25. Sheppard CJ. Fractal model of light scattering in biological tissue and cells. *Opt Lett.* 2007;32:142-144.
  26. Xu M, Alfano RR. Fractal mechanisms of light scattering in biological tissue and cells. *Opt Lett.* 2005;30:3051-3053.
  27. Schmitt JM, Kumar G. Turbulent nature of refractive-index variations in biological tissue. *Opt Lett.* 1996;21:1310-1312.
  28. Rogers JD, Capoglu IR, Backman V. Nonscalar elastic light scattering from continuous random media in the born approximation. *Opt Lett.* 2009;34:1891-1893.
  29. Yi J, Backman V. Imaging a full set of optical scattering properties of biological tissue by inverse spectroscopic optical coherence tomography. *Opt Lett.* 2012;37:4443-4445.
  30. Yi J, Radosevich AJ, Rogers JD, et al. Can OCT be sensitive to nanoscale structural alterations in biological tissue? *Opt Express.* 2013;21:9043-9059.
  31. Feng L, Zhao Y, Yoshida M, et al. Sustained ocular hypertension induces dendritic degeneration of mouse retinal ganglion cells that depends on cell type and location. *Invest Ophthalmol Vis Sci.* 2013;54:1106-1117.
  32. Radosevich AJ, Yi J, Rogers JD, Backman V. Structural length-scale sensitivities of reflectance measurements in continuous random media under the Born approximation. *Opt Lett.* 2012;37:5220-5222.
  33. Levkovitch-Verbin H, Quigley HA, Martin KR, Zack DJ, Pease ME, Valenta DF. A model to study differences between primary and secondary degeneration of retinal ganglion cells in rats by partial optic nerve transection. *Invest Ophthalmol Vis Sci.* 2003;44:3388-3393.
  34. Levkovitch-Verbin H, Quigley HA, Kerrigan-Baumrind LA, D'Anna SA, Kerrigan D, Pease ME. Optic nerve transection in monkeys may result in secondary degeneration of retinal ganglion cells. *Invest Ophthalmol Vis Sci.* 2001;42:975-982.
  35. Fitzgerald M, Bartlett CA, Harvey AR, Dunlop SA. Early events of secondary degeneration after partial optic nerve transection: an immunohistochemical study. *J Neurotrauma.* 2010;27:439-452.
  36. Li H, Liang Y, Chiu K, et al. Lycium barbarum (wolfberry) reduces secondary degeneration and oxidative stress, and inhibits JNK pathway in retina after partial optic nerve transection. *PLoS One.* 2013;8:e68881.
  37. Yoles E, Muller S, Schwartz M. NMDA-receptor antagonist protects neurons from secondary degeneration after partial optic nerve crush. *J Neurotrauma.* 1997;14:665-675.
  38. Cummins N, Bartlett CA, Archer M, et al. Changes to mitochondrial ultrastructure in optic nerve vulnerable to secondary degeneration in vivo are limited by irradiation at 670 nm. *BMC Neurosci.* 2013;14:98.
  39. Tezel G, Yang X, Yang J, Wax MB. Role of tumor necrosis factor receptor-1 in the death of retinal ganglion cells following optic nerve crush injury in mice. *Brain Res.* 2004;996:202-212.
  40. Leung CK, Lindsey JD, Crowston JG, Lijia C, Chiang S, Weinreb RN. Longitudinal profile of retinal ganglion cell damage after optic nerve crush with blue-light confocal scanning laser ophthalmoscopy. *Invest Ophthalmol Vis Sci.* 2008;49:4898-4902.
  41. Nickells RW. From ocular hypertension to ganglion cell death: a theoretical sequence of events leading to glaucoma. *Can J Ophthalmol.* 2007;42:278-287.

42. Li HY, Ruan YW, Ren CR, Cui Q, So KF. Mechanisms of secondary degeneration after partial optic nerve transection. *Neural Regen Res.* 2014;9:565-574.
43. Dubra A, Sulai Y. Reflective afocal broadband adaptive optics scanning ophthalmoscope. *Biomed Opt Express.* 2011;2:1757-1768.
44. Li H, Lu J, Shi G, Zhang Y. Measurement of oxygen saturation in small retinal vessels with adaptive optics confocal scanning laser ophthalmoscope. *J Biomed Opt.* 2011;16:110504.
45. Spicer GL, Azarin SM, Yi J, et al. Detection of extracellular matrix modification in cancer models with inverse spectroscopic optical coherence tomography. *Phys Med Biol.* 2016;61:6892-6904.